ELSEVIER

Tectonophysics 324 (2000) 1–16

TECTONOPHYSICS

www.elsevier.com/locate/tecto

Shear test results for cohesion and friction coefficients for different granular materials: scaling implications for their usage in analogue modelling

W.P. Schellart *

Epsilon Laboratory, Australian Crustal Research Centre, Department of Earth Sciences, PO Box 28E, Monash University, Melbourne VIC 3800, Australia

Received 21 December 1999; accepted for publication 28 April 2000

Abstract

Laboratory tests have been carried out on dry granular materials such as quartz sand, glass microspheres and sugar with different grain size, rounding and sphericity. The measurements have been made with a simple shear test machine for different values of normal stress (~50–900 Pa). Shear stress has been plotted against normal stress in order to determine the cohesion and coefficient of internal friction for the investigated materials.

Resulting values of cohesion and coefficient of internal friction are mainly dependent on rounding and sphericity, while grain size has a less significant influence. Further, the behaviour of the materials for very small normal stresses (~0–400 Pa) is more complex than previously assumed. The fracture envelopes for all materials investigated are convex-outward for this small range and converge towards a straight failure envelope with increasing normal stress. Finally, in extensional faulting experiments, there is no significant change in fault dip with increasing depth. Therefore, the non-linear behaviour for small normal stresses is best described as a dependence of the cohesion on the normal stress and not as a dependence of the coefficient of internal friction on the normal stress. Values for cohesion increase from ~0 Pa (±15 Pa) at zero normal stress to 137–247 Pa (±15 Pa) for normal stresses greater than ~250–400 Pa. The results show that well-rounded, spherical material is better suited to model brittle behaviour of rocks in crustal and lithospheric scale analogue models than less well-rounded material, since it has a smaller cohesion and a coefficient of internal friction, which is closer to values of natural rocks.

Keywords: analogue modelling; coefficient of internal friction; cohesion; granular material; normal stress; shear stress

1. Introduction

Dry granular materials such as sand have been previously used in many analogue models of structural and tectonic processes (Hubbert, 1951; Horsfield, 1977; Naylor et al., 1986; Vendeville et al., 1987; Davy and Cobbold, 1988, 1991; McClay, 1990; Ratschbacher et al., 1991; Richard, 1991; Richard and Krantz, 1991; Richard et al., 1991, 1995; Lallemand et al., 1992; Nieuwland and Walters, 1993; Brun et al., 1994; Faccenna et al., 1996, 1999; Bonini et al., 1997; Hatzfeld et al., 1997; Keep and McClay, 1997; Basile and Brun, 1998). In most of these papers, the cohesion of these

* Fax: +61-3-9905-4903.
E-mail address: wouter@mail.earth.monash.edu.au (W.P. Schellart)

0040-1951/00/$ - see front matter
PII: S0040-1951(00)00111-6

Nomenclature

σ_{ij}	stresses (Pa)
C	cohesion (Pa)
ρ	density (kg/m^3)
x_j	length vector (m)
σ_1	maximum principal stress (Pa)
σ_3	minimum principal stress (Pa)
β	parameter depending on the type of faulting
g	acceleration due to gravity (m/s^2)
z	depth below surface (m)
λ	pore fluid factor
τ	shear stress (Pa)
σ_n	normal stress (Pa)
S	fracture strength under uniaxial compression and zero confining pressure (Pa)
K	parameter related to fracture angle
θ_f	fracture angle
ϕ	angle of internal friction
μ	coefficient of internal friction
m	mass of shear load (kg)
A	area of fault surface (m^2)
h	thickness of sandpack above the gap (m)
x^*	critical point defined by σ_n^* and τ^*
σ_n^*	critical normal stress, below which the relation between σ_n and τ is non-linear (Pa)
τ^*	critical shear stress, below which the relation between σ_n and τ is non-linear (Pa)
C'	maximum extrapolated cohesion (Pa)

materials has been assumed to be negligible and the coefficient of internal friction to be $\sim$0.58. However, shear test measurements done by Krantz (1991) revealed that the cohesion of sand is probably in the order of 300–520 Pa (depending on the physical handling technique), which is certainly not negligible. Further, the coefficient of internal friction is in the order of 0.58–1.00. These values could, however, be subject to an error due to extrapolation of data towards very small normal stresses (0–600 Pa), as has been suggested by Krantz (1991) and Richard and Krantz (1991). Recently, Cobbold and Castro did shear tests for normal stresses ranging from 300–1600 Pa. They obtained an extrapolated cohesion of 85 Pa for the material and a coefficient of internal friction of 0.57. Cobbold and Castro (1999) also did shear tests with upward fluid flow through the material, leading to effective normal stresses of 0–1600 Pa. They also fitted straight lines to the data resulting from these experiments. However, it would have been possible to fit more complex envelopes to these data sets, especially near the origin.

Analogue experiments are subject to specific scaling rules, which were introduced to geology by Hubbert (1937). According to these scaling rules, an analogue model is representative of a natural prototype if both systems are dynamically similar. This means that in both experiment and nature, similar distributions of stresses, densities and rheologies should be present. In analogue modelling of structural and tectonic processes, cohesion should scale down in a similar way to how stresses scale down (Horsfield, 1977; Davy and Cobbold, 1988; Cobbold and Jackson, 1992). When analogue experiments are executed in a normal field of gravity, stresses should be scaled down as the product of density and length vectors scales down:

$$\frac{C^a}{C^n} = \frac{\sigma_{ij}^a}{\sigma_{ij}^n} = \frac{\rho^a x_j^a}{\rho^n x_j^n} \tag{1}$$

where superscript a denotes the analogue model

and superscript n the natural prototype; C is the cohesion; σ_{ij} are the stresses; ρ is the density; and x_j is a length vector.

If a scale factor of 5×10^{-7} is applied to stresses (with a density ratio of 1/2 and a length ratio of 1 cm/10 km), the implied cohesion values in the natural system are in the range of 600–1040 MPa. That is of course when the values for cohesion of Krantz (1991) are correct. These upscaled values are extremely high and unrealistic values for natural rocks. Uniaxial compressive strength tests and shear strength tests on natural rocks have indicated that values for cohesion of intact rocks range between ~20–110 MPa. Several values of cohesion and coefficient of internal friction for intact sedimentary and igneous rocks can be observed in Table 1.

As most rocks are broken by numerous joints, faults and fractures, at least on a larger scale compared to the test specimens investigated in these tests (Hubbert, 1951), the cohesion of natural rocks will probably be even lower than the values given in Table 1.

Also, in lithospheric modelling, some people assume that the cohesion for the upper (brittle) part of the lithosphere is negligible since they apply the following equation for this brittle behaviour (Sibson, 1974):

$$\sigma_1-\sigma_3\geq\beta\rho gz(1-\lambda) \tag{2a}$$

where σ_1 and σ_3 are the maximum and minimum principal stress, respectively; β is a parameter depending on the type of faulting (3, 1.2 and 0.75 for thrust, strike-slip and normal faulting, respectively); g is the acceleration due to gravity; z is the depth below the surface; and λ is the pore fluid factor.

This assumption of negligible cohesion is mainly based on the idea that the upper part of the crust is crisscrossed by discontinuities of every shape and size (Ranalli and Murphy, 1987). This statement could be true for the continental lithosphere, which normally has experienced major deformation events. However, this statement is probably less valid for the oceanic lithosphere, where intensive deformation is absent, and the only major faults are transform faults offsetting different mid oceanic ridge segments.

Another equation that is often used for plots of lithospheric strength profiles is that proposed by Byerlee (1978):

$$\tau=0.85\sigma_n \quad \text{for } \sigma_n<200 \text{ MPa} \tag{2b}$$

$$\tau=60 \text{ MPa}+0.6\sigma_n \quad \text{for } 200<\sigma_n<1700 \text{ MPa} \tag{2c}$$

where τ is the shear stress, and σ_n is the normal stress.

When Eqs. (2b) and (2c) are rewritten in terms of principal stresses (Kirby, 1983), this leads to:

$$\sigma_1-\sigma_3=3.9\sigma_3 \quad \text{for } \sigma_3<120 \text{ MPa} \tag{2d}$$

$$\sigma_1-\sigma_3=210 \text{ MPa}+2.1\sigma_3 \quad \text{for } \sigma_3>120 \text{ MPa}. \tag{2e}$$

The equations of Byerlee (1978) have been empirically determined from numerous experiments on shear strength along fracture planes of various types of prefractured rocks. From Eq. (2b), it can be observed that prefractured rocks have essentially no cohesion along their fracture planes for this small stress range. However, for increasing normal pressure, Eq. (2c) shows that prefractured rocks do have a cohesion of 60 MPa. According to Byerlee (1978), this difference is related to

Table 1
Values of μ (coefficient of internal friction), ϕ (angle of internal friction) and C (cohesion) for different rock types[a]

Rock type	μ	ϕ	C (MPa)	Reference
Granite	0.64	32.6	31	1
Gabbro	0.66	33.4	38	1
Trachyte	0.68	34.2	41	1
Serpentinized olivine	0.65	33.0	90	2
Sandstone	0.51	26.6	28	1
Berea sandstone	0.49	26.1	24	3
Weber sandstone	0.60	31.0	70	3
Tennessee sandstone	0.84	40.0	50	4
Lueders limestone	0.53	27.9	15	4
Solnhofen limestone	0.53	27.9	105	4
Marble	0.75	36.9	110	1
Blair dolomite	1.00	45.0	45	4

[a] References: 1: Jaeger and Cook (1976); 2: Raleigh and Paterson (1965); 3: Twiss and Moores (1992); 4: Handin (1969).

different physical mechanisms involved in the sliding of rock at various pressures. At low normal stresses, the surfaces can move with respect to one another by lifting over the interlocked irregularities, while at high normal stresses, this effect is suppressed, and the surfaces then slide by shearing through the irregularities.

However, since analogue models of the crust and lithosphere have been made, where the (upper) brittle part of the crust has been simulated with pure sand (Brun et al., 1994; Bonini et al., 1997; Basile and Brun, 1998), or sand mixed with a certain amount of ethyl cellulose (Davy and Cobbold, 1988, 1991; Ratschbacher et al., 1991; Cobbold and Jackson, 1992; Faccenna et al., 1996; Hatzfeld et al., 1997), the cohesion of these materials could have a major effect on the strength profiles through the model crusts and lithospheres. The inclusion of cohesion in the analogue models may lead to integrated strengths, which are too large for the brittle upper part of the lithosphere. The lithospheric strength can be plotted by the following formula, which is a form of Coulomb's fracture criterion (Coulomb, 1773) rewritten in terms of principal stresses:

$$\sigma_1-\sigma_3=(K-1)\rho gz(1-\lambda)+S \quad \text{(shortening)} \tag{3a}$$

$$\sigma_1-\sigma_3=\frac{(K-1)}{K}\rho gz(1-\lambda)+\frac{S}{K} \quad \text{(extension)} \tag{3b}$$

with:

$$S=\frac{2C\sin 2\theta_f}{1+\cos 2\theta_f} \quad K=\frac{1-\cos 2\theta_f}{1+\cos 2\theta_f} \tag{3c}$$

and

$$2\theta_f=90+\phi \quad \mu=\tan\phi \tag{3d}$$

where K is a parameter depending on the fracture angle; S is the fracture strength under uniaxial compression with zero confining pressure; θ_f is the fracture angle; ϕ is the angle of internal friction; and μ is the coefficient of internal friction.

A strength curve for sand (shortening) can be plotted, using Eq. (3a) with a coefficient of internal friction $\mu=0.58$ and a cohesion $C=0$ Pa, as assumed by most analogue crustal scale and lithospheric modellers (Davy and Cobbold, 1988, 1991; Ratschbacher et al., 1991; Cobbold and Jackson, 1992; Brun et al., 1994; Faccenna et al., 1996; Bonini et al., 1997; Basile and Brun, 1998). When this is compared with a strength curve for poured sand with $C=300$ Pa and $\mu=0.58$ and sprinkled sand with $C=520$ Pa and $\mu=1.00$ [as deduced by Krantz (1991)], the difference in integrated strength is very large (Fig. 1).

For the first 10 mm, the integrated strength for curve I is $\sim$1.4 N/m and for curve III $\sim$28.4 N/m, which differ by a factor 20. The integrated strength for the first 20 mm for curve I is $\sim$5.5 N/m and for curve III $\sim$63.5 N/m, which is still different by a factor 11. This indicates that if the calculated values for cohesion and angle of internal friction of Krantz (1991) are correct, the integrated strength of sand does not scale properly to repre-

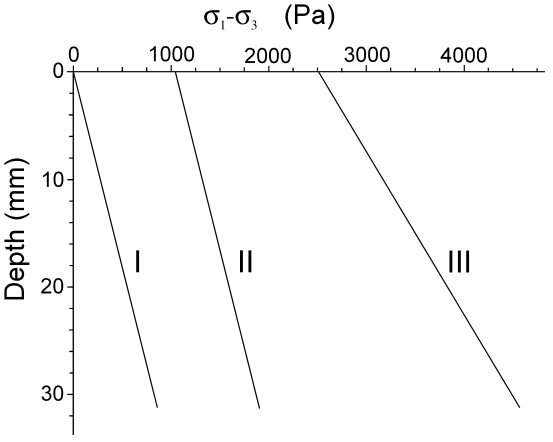

Fig. 1. Brittle failure curves of dry granular materials for shortening. All three curves are for material with a frictional plastic behaviour, with a pore fluid factor $\lambda=0$. For convenience, a constant density (ρ) of 1400 kg/m^3 for all three curves has been chosen. Curves with different values for K (related to the coefficient of internal friction μ) and S (related to cohesion C and μ) have been plotted. For curve I, the fracture strength $S=0$ Pa and $K=3.00$, for curve II $S=1042$ Pa and $K=3.00$ and for curve III $S=2511$ Pa and $K=5.83$. The three different curves clearly indicate that cohesion as well as the coefficient of internal friction have a major influence on the strength of the material and therefore on the integrated strength profiles for lithospheric analogue models.

sent the lithosphere, at least when a scaling factor of $<5\times10^{-6}$ is applied to the analogue model.

However, since the experiments of Krantz (1991) have been executed with normal stresses varying somewhere between 600 and 3500 Pa and his data have been extrapolated to normal stresses of 0–600 Pa, this extrapolation might lead to errors and therefore incorrect strength curves. Normally, sand layers used in lithospheric analogue models have thicknesses smaller than a few centimetres, leading to vertical normal stresses of up to only a few hundred Pascals. Therefore, shear test experiments reported here have been executed for very low normal stresses (50–900 Pa). The aim of these experiments is to obtain a better picture of the dynamic behaviour of sand and other granular materials in this low normal stress range and to investigate which material is most suitable for future analogue modelling of the lithosphere.

2. Measurements

For a frictional plastic material (such as pure sand and glass microspheres), it is important to know its cohesion since its inherent shear strength is dependent on it. This dependence can be observed in Coulomb's fracture criterion (Coulomb, 1773):

$$\tau = C + \mu\sigma_{\mathrm{n}}. \tag{4}$$

To determine the cohesion from a granular material (which probably has a very small or even zero cohesion), it is important to measure the relationship between the shear stress (which leads to fracturing) and the normal stress when the normal stress is as small as possible, to minimize the uncertainty of extrapolations to zero normal stress.

Shear strengths can be measured using a Hubbert-type apparatus (Hubbert, 1951). Here, an upper ring is suspended above a fixed lower ring, with a small gap in between (Fig. 2).

The lower and upper rings are filled with the material under investigation to a desired depth (h). On the upper suspended ring an increasing shear load is applied until failure occurs in the material, which results in a significant displacement of the upper ring. This displacement was limited by a mechanical stop to approximately 4 mm.

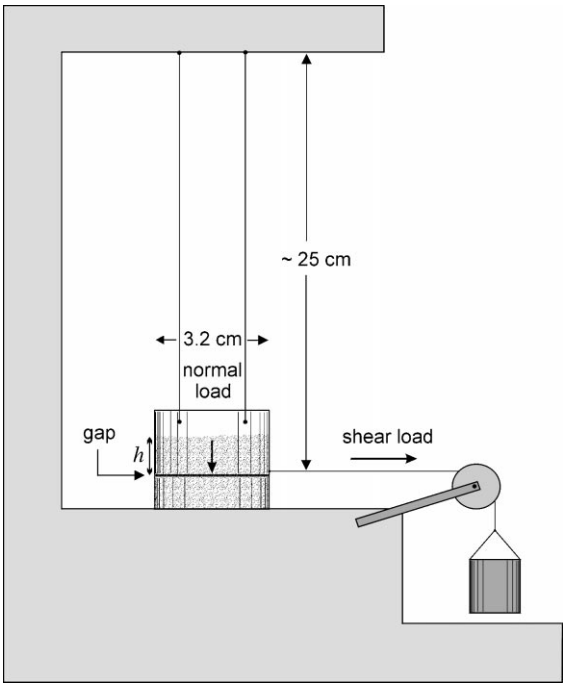

Fig. 2. Sketch of shear test apparatus. The upper ring is suspended above a fixed lower ring with a gap of $\sim$0.3 mm in between. After filling the rings to a desired depth (h), measured from the gap (the future fault zone), an increasing shear load is applied by a mass hanging over a pulley until failure occurs. This mass is essentially an empty bucket, which can be filled gradually with sand.

A few modifications to this apparatus have been applied, as carried out by Krantz (1991). The first modification is that the suspension of the upper ring was nearly 25 cm in length (or about eight times the diameter of the rings) to reduce the friction of the apparatus itself. The second modification is that the normal stress on the horizontal fault surface was determined only by the thickness of the overlying sandpack (h).

Further, a modification on the apparatus of Krantz (1991) has been applied, i.e. the rings that have been used have a much smaller diameter (3.2 cm) than the rings in his apparatus (14 cm). This has been done in order to be able to make the sediment thickness in the upper ring as small and as constant as possible. With this experimental

set-up, it was possible to execute experiments with normal stresses in the range of 50–900 Pa.

A few things should be taken into consideration in order to minimize any errors in the measurements. First of all, the friction of the pulley and the suspended ring should be taken into consideration. The friction of the total system has been measured by investigating the amount of mass needed to significantly displace the upper suspended (empty) ring. It has been found that a shear stress as small as 3.0 Pa was sufficient to displace the upper suspended ring some 3 mm. The error in shear stress induced by this friction is thus in the order of only a few Pascals, and since the shear stresses in the experiments range between 100 and 1000 Pa, this leads to a maximum error of a few per cent.

Further, the friction between the sediment and the upper suspended ring should be taken into consideration. If this force is very large, then it will inhibit the grains to fall freely and therefore will reduce the normal stress of the sediment load. This possible influence of such a force has been checked by weighing the mass of the sediment, while supported by the suspended upper ring and comparing it with the mass of the sediment, when the suspended ring was removed. It was found that this force was less than 0.5%.

Also, it is important to prepare the material for every experiment with a uniform method, since density and coefficient of internal friction of the material are dependent on the physical handling technique (Krantz, 1991). The experiments of Krantz (1991) revealed that density, cohesion and coefficient of internal friction increase significantly when granular material is sprinkled instead of rapidly poured. In all the following shear test experiments, the test material has been slowly poured from a uniform height of ~ 10 cm.

Finally, with a very small sediment thickness, it is important that the fault plane in the sediment runs according to the plane defined by the gap between the two rings. In most experiments with a very small sediment thickness ($\sim < 0.5$ cm), the fault plane had an inclined angle to the horizontal (small thrust fault). The results from experiments where thrust faults developed have been rejected.

The shear stress is related to the mass of the shear load and the area of the fault plane, and the normal stress is related to the thickness of the sandpack (h) and the density of the material. The shear stress and the normal stress have been calculated with the following equations:

$$\tau = \frac{mg}{A} \tag{5a}$$

$$\sigma_n = \rho g h \tag{5b}$$

where m, A and h are the mass of shear load, the area of the fault surface and the thickness of the sandpack (with respect to the gap), respectively.

By plotting the shear stress, necessary to induce horizontal faulting, versus different normal stresses (by varying the height, h, of the sediment column), a curve can be obtained. Here, the intersection of this curve with the shear stress axis ($\sigma_n = 0$ Pa) is the cohesion of the material, and the slope of the curve is the coefficient of internal friction.

With a ring diameter of 3.2 cm, the area of the future fault surface is $\sim 8.0 \times 10^{-4}$ m^2. The acceleration due to gravity, g, was taken as 9.8 m/s^2.

For each material, at least 70 shear tests were carried out, with values for the height of the sediment column (h) in the range of 0.5–5.0 cm.

Also, a few experiments were recorded with a digital video camera, in order to investigate the experiments at different increments of time during shearing. The camera shot 25 images per second, where every image was shot over a time lapse of 1 ms.

3. Materials

In the shear tests, only dry granular materials have been examined. Dry granular materials such as sand exhibit frictional plastic behaviour and fail according to the Mohr–Coulomb failure criterion (Hubbert, 1951; Mandl et al., 1977). Dry sand (S), glass microspheres (GM) and caster sugar (CS) with different grain sizes have been examined. The materials that have been investigated and some of their physical properties (density, grain size, roundness, sphericity) are listed in Table 2. The roundness of the materials has been classified using the classification of Powers (1953).

Table 2
Material properties of materials used in the shear test experiments, where 'S' stands for sand, 'GM' for glass microspheres and 'CS' for caster sugar[a]

Material	Density (kg/m^3)	Grain size (μm)	Roundness	Sphericity
S I	1731	<400	(Sub)angular	Intermediate
S II	1674	90–180	(Sub)angular	Intermediate
GM I	1905	400–600	Very well rounded	Very high
GM II	1609	90–180	Well rounded	High
CS	1044	<355	Angular	Low

[a] The error in density is ±2%.

Sphericity has been determined by dividing the shortest axis of the grain by its longest axis. Where most grains had numbers smaller than 0.5, the sphericity has been classified as low, for numbers between 0.5 and 0.8, the sphericity has been classified as intermediate, and for numbers higher than 0.8 the sphericity has been classified as high.

The grain size has been determined using sieves with different mesh sizes. The density of the materials has been determined by measuring the mass of known volumes of the material with an electronic balance.

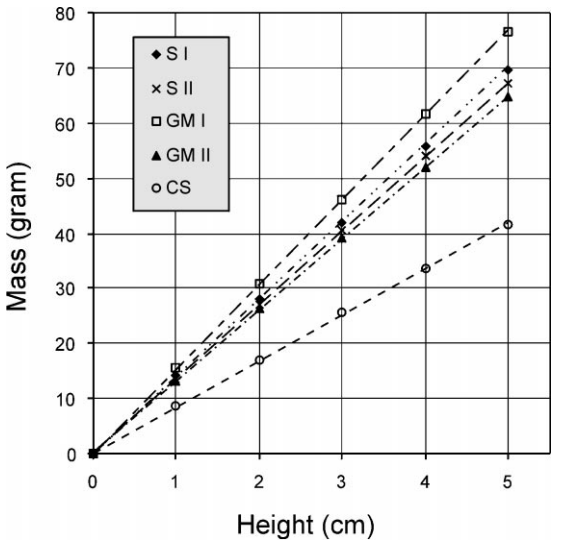

Fig. 3. Plot of data displaying the relationship between increase in mass and increase in height of the sediment column (h) for the investigated materials. Dashed lines are best-fit straight lines for the data. From these results, it can be seen that compaction does not influence density significantly for such small sediment thicknesses.

The mass has been determined for five different volumes in the upper suspended ring, with a thickness (h) increasing from 1 to 5 cm. This has been done to determine whether there would be any increase in density for increasing thickness of the sediment column due to compaction. For the materials investigated, the measurements gave almost perfectly linear results (Fig. 3), suggesting that compaction in this range due to increasing normal stress is absent, as has also been recovered by Cobbold and Castro (1999).

4. Results

The results of the shear tests have been plotted in Fig. 4a. Approximate best-fit lines for the data have been plotted in Fig. 4b. Here, it can be observed that, if no data were present for normal stresses, lower than 400 Pa, extrapolation of the data would lead to estimated values for cohesion, which would be much too high for the normal stress range of 0–400 Pa. Further, it can be observed that sphericity and rounding seem to have more effect on the shape and position of the curve than grain size.

The data sets for each material strongly suggest convex-outward envelopes for normal stresses below ~250–400 Pa and shear stresses below ~300–550 Pa, with a non-linear relationship between τ and σ_n (Fig. 4a). Above these values, the relationship between τ and σ_n shows normal Coulomb behaviour, as defined by Eq. (4). Approximate values of μ, ϕ and C' (maximum extrapolated cohesion) for the data in the range $\sigma_n > 250$–400 Pa are listed in Table 3. Further, it

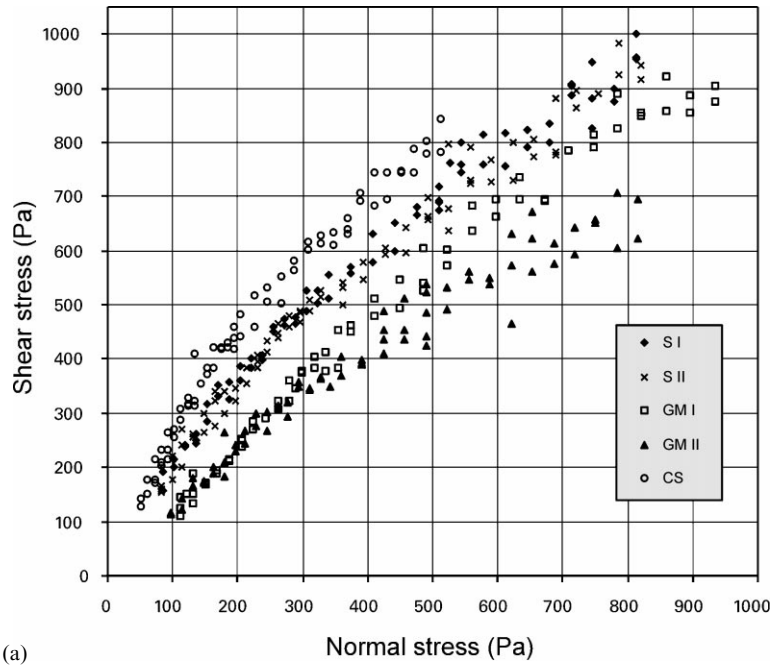
Shear stress (Pa)
Normal stress (Pa)
0
100
200
300
400
500
600
700
800
900
1000
S I
S II
GM I
GM II
CS

(a)

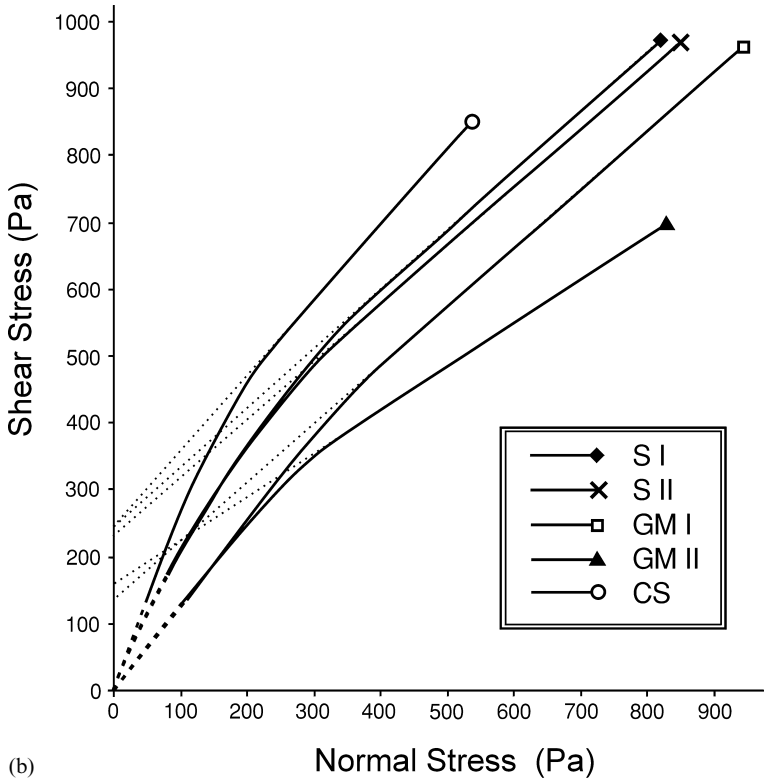
Shear Stress (Pa)
Normal Stress (Pa)
0
100
200
300
400
500
600
700
800
900
1000
S I
S II
GM I
GM II
CS

(b)

Table 3
Values for μ (coefficient of internal friction), ϕ (angle of internal friction) and C′ (maximum extrapolated cohesion), all for the linear part of the failure envelopes for the investigated materials[a]

Material	μ	ϕ	C' (Pa)
S I	0.89	41.7	245
S II	0.88	41.3	230
GM I	0.87	41.0	137
GM II	0.65	33.0	160
CS	1.14	48.8	247

[a] Errors in the data are in the order of 5%.

can be observed that for $\sigma_n < 250$–400 Pa, the data converge towards the origin, indicating that at zero normal stress, the cohesion of all the granular materials is 0 Pa (± 15 Pa), as has been suggested earlier by Richard and Krantz (1991).

From the individual experiments and careful investigation of some of the experiments, recorded with a video camera, it has been observed that rupture (which led to a significant displacement of more than 3 mm) was preceded by one or two microslips. These microslips were most evident for experiments with S I, S II and CS and least evident with GM I. In most recorded experiments, the first microslip was smaller ($\sim$0.1–0.2 mm) than the second ($\sim$0.2–0.3 mm).

Further, dilatancy of the fault zones has been observed during and after the experiments, as mentioned by Mandl et al. (1977) and Mandl (1988). After rupture, the sediment in the upper suspended ring was uplifted with respect to this ring, compared to the stage before rupture. This uplift was maximum and approximately 1 mm for small sediment columns ($h \sim 0.5$–0.6 cm) and decreased gradually to 0 mm for larger sediment columns ($h \sim 1.3$–2.0 cm). This decrease in uplift is probably related to the increase in normal stress on the fault plane, and therefore, dilatancy of fault zones in dry granular materials probably decreases with increasing depth. It has also been observed that the uplift decreases with decreasing grain size, uplift values for S II and GM II being approximately half as large as those for S I, GM I and CS. The decrease in dilatancy of the shear zones with increasing normal stress could be related to the convex-outward behaviour of the envelopes at low normal stresses, since the normal stresses, where this dilatancy becomes negligible (250–350 Pa), coincide approximately with the normal stresses at the point where the envelopes become more or less straight (250–400 Pa). A possible explanation for the decrease in dilatancy in these shear zones is that different physical mechanisms operate at different normal stresses. For low normal stresses, the individual grains in a shear zone can move over one another, leading to dilatation of the shear zone and uplift of the sediment column. For high normal stresses, this effect is suppressed, and the individual grains have to slide through the irregularities. This concept has already been proposed by Byerlee (1978), for shearing along fracture planes in rocks.

Finally, from the recorded experiments, there were strong indications that during the major shear events, the shears grew from the back of the ring towards the front because the uplift of the sediment column started in the back and progressively migrated towards the front of the ring (where the ring is attached to the shear load). The development of these shears normally took approximately 0.05–0.1 s.

When starting at the origin, with increasing normal stress, the failure envelopes are convex-outward and converge towards the straight curve until they reach a critical point x^*, which is defined by its critical normal and shear stress (σ_n^*, τ^*). From this critical point, with increasing normal stress, the curve is more or less straight. The non-linear behaviour below this critical point x^* could

Fig. 4. (a) Shear stress plotted as a function of normal stress for different dry granular materials. Material properties for the different materials have been given in Table 2. (b) Approximate best-fit envelopes for the data of the materials plotted in (a). Continuous lines are for regions, where data are present, dashed lines are extrapolated for very low normal stresses ($<$50–100 Pa), and stippled lines are extrapolated lines, when no data for normal stresses lower than $\sim$250–400 Pa are included. The intersection of these stippled lines with the shear stress axis gives the maximum extrapolated cohesion, C'.

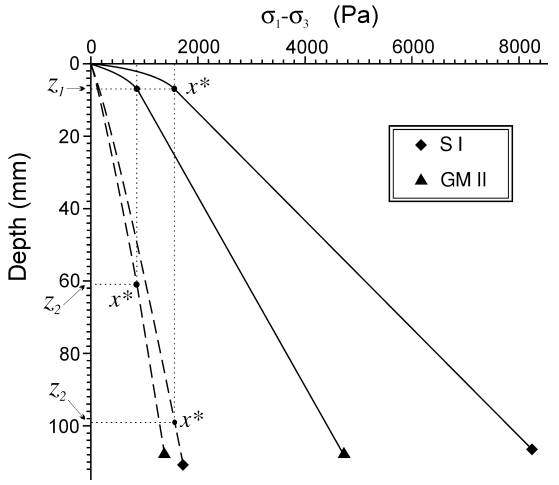

Fig. 5. Brittle failure curves of S I and GM II for shortening (continuous lines) and extension (dashed lines). From the curves, it is evident that the critical point x^* has a much greater critical depth value in extension (z_2) than in shortening (z_1). Further, it can be seen that the stress value for x^* ($\sigma_1-\sigma_3$) is the same in both cases, as would be suspected from Fig. 6.

be described as a dependence of C on σ_n and/or μ on σ_n:

$$C=f(\sigma_n) \quad \text{and/or } \mu=g(\sigma_n). \tag{6}$$

Before investigating which of these factors influences the behaviour of the curves below x^*, we will transform these curves in terms of principal stresses and burial depth [a standard $\sigma_1-\sigma_3$ versus burial depth (z) plot]. This transformation has been executed for both shortening and extension. The resulting curves for S I and GM II are plotted in Fig. 5. Here, it can be observed that the critical point has a much higher z value in extension than in shortening.

The dependence of the critical depth, z, on the type of deformation (shortening or extension) can be explained by plotting a Mohr circle, which makes contact with the envelope at the critical point x^* (Fig. 6). For shortening, σ_1 is the horizontal stress and σ_3 the vertical stress. For extension, it is just the opposite. Since vertical stress is approximated by the following equation:

$$\sigma_{\text{vertical}}=\rho g z. \tag{7}$$

then for shortening at the critical point:

$$\sigma_{\text{vertical}}=\sigma_3=\rho g z_1. \tag{8a}$$

For extension at the critical point:

$$\sigma_{\text{vertical}}=\sigma_1=\rho g z_2. \tag{8b}$$

Dividing Eq. (8a) by Eq. (8b) leads to:

$$\frac{\sigma_3}{\sigma_1}=\frac{\rho g z_1}{\rho g z_2}=\frac{z_1}{z_2}\ \begin{matrix}\text{(shortening)}\\ \text{(extension)}\end{matrix} \tag{9}$$

since gravity and density are the same in both cases. From this relation, it is clear that the depth of x^* in extension (z_2) is greater than its depth in shortening (z_1).

We will now return to the question of which factor in Eq. (6) influences the non-linear behaviour of the envelope. If μ is a function of σ_n, the angle of internal friction ϕ should decrease with depth. In an extensional setting (where σ_1 is vertical), this would lead to a decreasing dip angle of normal faults with depth.

For example, for the material S I, this would lead to a dip angle of $\sim 80^\circ$ in the uppermost few centimetres, decreasing progressively to $\sim 66^\circ$ at $z=z_2$.

The possible dependence of μ on σ_n has been investigated in a small number of extensional experiments. The experiments have been performed in laterally unconfined piles of sediment for the materials S I and GM II, since lateral confinement increases fault dips at the edges due to extra frictional resistance (Hubbert, 1951; Krantz, 1991). The sediment piles rested on a flat basal plate with, on one side, a thin plastic sheet in between the sediment pile and the basal plate. During an experiment, the plastic sheet was moved laterally outward, perpendicular to its straight edge, where the lateral displacement was no bigger than required to produce a visible fault scarp. To investigate the possible dependence of μ with respect to the burial depth, the thickness of the sediment pack was varied (2, 4, 6, 8 and 10 cm). For instance, this results in a normal stress range along the fault plane of 0 to ~ 31 Pa (S I) or 0 to ~ 72 Pa (GM II) for a 2 cm thick sediment pack. For a 10 cm thick sediment pack, this results in a normal stress range along the fault plane of 0 to ~ 365 Pa (S I) or 0 to ~ 580 Pa (GM II).

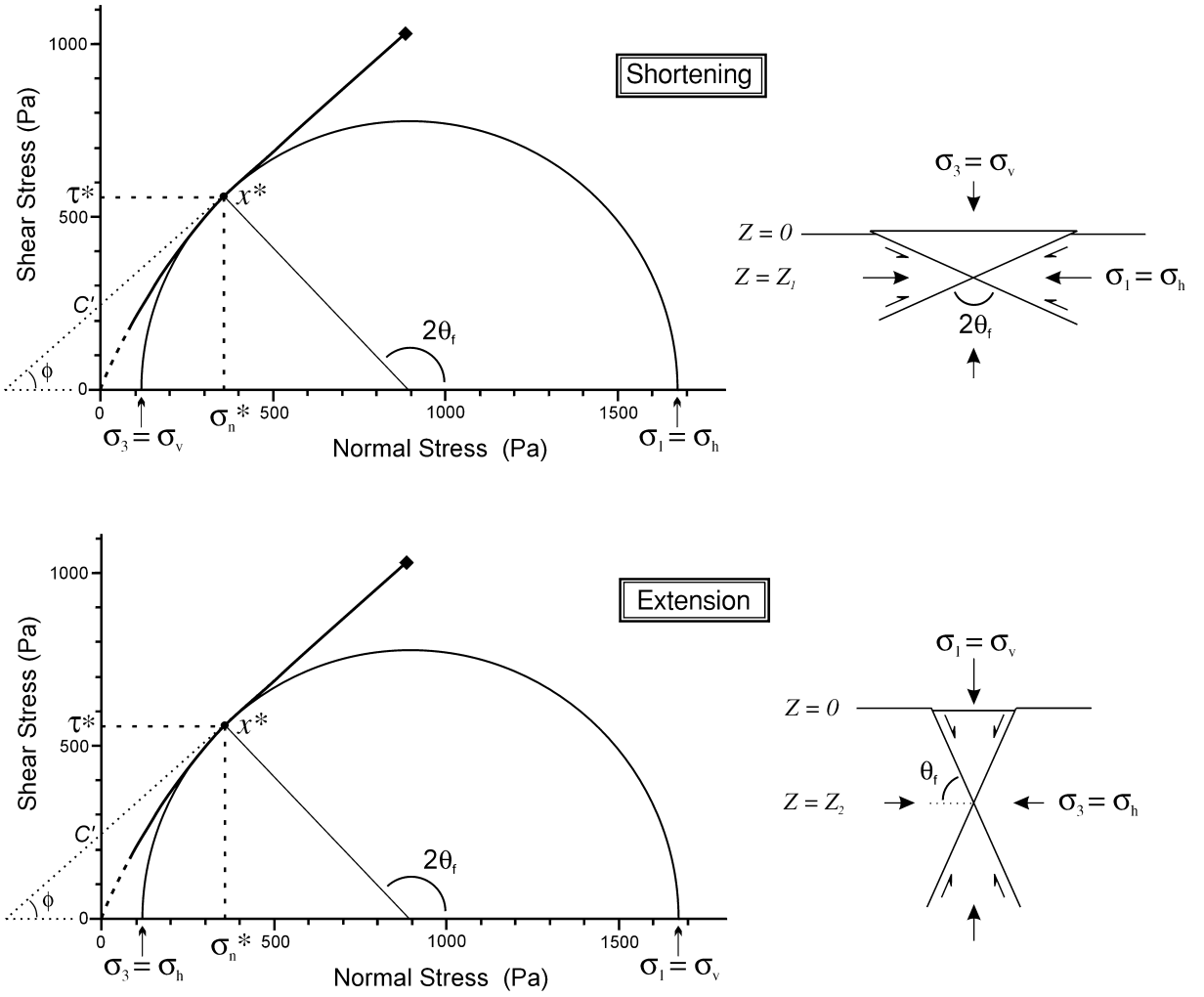

Fig. 6. Mohr diagram and failure envelope for S I. Failure occurs at the critical point, x^*, for a critical normal stress and shear stress, with accessory values for σ_1 and σ_3. For shortening, the critical point will be reached at a depth z_1 and for extension, the critical point will be reached at a depth z_2, with $z_1 < z_2$.

Measurements have been made for both rapidly poured sand and sprinkled granular material.

During every experiment, a symmetric graben developed, where a synthetic and an antithetic fault developed simultaneously. The fault scarps were approximately of constant strike.

The fault dip has been determined by taking the inverse tangent of the thickness of the sediment pack, divided by half the width of the graben, assuming that it is constant with depth. Since the maximum principal stress in these extensional experiments is vertical, the relationship between the dip of the fault plane, the fracture angle (θ_f) and the angle of internal friction (ϕ) can be written as follows:

$$\text{fault dip} = \theta_f = 45^\circ + \frac{\phi}{2}. \tag{10}$$

The fault dips obtained from the experiments and the calculated angles of internal friction are given in Table 4.

Table 4
Fault dip angles and angles of internal friction ϕ for different thicknesses of the sediment packs for the materials S I and GM II (for both pouring and sprinkling of the sediment)[a]. From these results, it is clear that there is little or no dependence of μ on σ_n

Thickness (cm)	Fault dip angle				Angle of internal friction (ϕ)			
	S I		GM II		S I		GM II	
	Poured	Sprinkled	Poured	Sprinkled	Poured	Sprinkled	Poured	Sprinkled
2	59.9	69.8	58.8	65.9	29.9	49.6	27.6	41.8
4	59.5	70.3	60.0	65.5	28.9	50.5	30.0	41.1
6	58.3	70.8	59.0	66.2	26.5	51.7	27.9	42.4
8	60.9	69.5	60.1	66.0	31.8	49.0	30.1	42.0
10	61.4	70.0	60.5	67.3	32.8	50.0	31.0	44.5

[a] The error in fault dip angle is $\pm 3^\circ$.

The dip angles in Table 4 validate the assumption of constant dip with increasing depth and therefore indicate that there is no dependence of μ on the burial depth, at least for this small range. Thus, there is no indication of a dependence of μ on σ_n. Therefore, the non-linear behaviour of the failure envelopes for very small normal stresses is best described as a dependence of the cohesion C on σ_n. From Table 4, it can also be observed that the use of a different physical handling technique to deposit the sediment piles has a major influence on the angle of internal friction, as has been noted earlier by Krantz (1991).

The calculated values for ϕ in Table 3 lie somewhere in between the obtained values for ϕ for pouring and sprinkling of the sediment in Table 4. This could be related to the slight difference in the physical handling technique for the sediment in the shear test experiments or to the inexact approximation of the normal and shear stress in these shear tests by using Eqs. (5a) and (5b).

5. Discussion

The shear tests pointed to non-linear convex-outward behaviour in normal versus shear stress diagrams for all granular materials investigated, for normal stresses smaller than $\sim$250–400 Pa and approximate linear behaviour for higher normal stresses (Fig. 4a and b). The values of cohesion for all the investigated materials are approximately 0 ($\pm$15 Pa) for $\sigma_n = 0$ Pa and gradually increase to 137–247 ($\pm$15 Pa) for $\sigma_n >$ 250–400 Pa.

This non-linear behaviour of the envelopes below a critical normal stress is not the result of a dependence of the coefficient of internal friction μ on σ_n, but may be represented as a dependence of the cohesion C on σ_n. This conclusion has been drawn because no change in fault dip with increasing burial depth (and thus increasing normal stress) has been observed in the extensional experiments (Table 4).

The obtained envelopes for the investigated materials may be represented by the following equations:

$$\tau = f(\sigma_n) + \mu\sigma_n \quad \text{for } 0\ \text{Pa} \le \sigma_n < \sigma_n^* \tag{11a}$$

$$\tau = C' + \mu\sigma_n \quad \text{for } \sigma_n \ge \sigma_n^*. \tag{11b}$$

An approximate representation of the curves for $0\ \text{Pa} < \sigma_n < \sigma_n^*$ might be a straight line. This results in:

$$\tau = \frac{\sigma_n}{\sigma_n^*} C' + \mu\sigma_n \quad \text{for } 0\ \text{Pa} \le \sigma_n < \sigma_n^* \tag{12a}$$

$$\tau = C' + \mu\sigma_n \quad \text{for } \sigma_n \ge \sigma_n^* \tag{12b}$$

These equations show a close resemblance to the eqs. (2b) and (2c) of Byerlee (1978). However, caution should be taken since his equations are deduced from experiments on prefractured rocks, while Eqs. (12a) and (12b) are representative for undeformed (dry granular) material.

Plotting curves for Eqs. (12a) and (12b) in a diagram would reveal two straight intersecting lines with different slopes. Here, the slope of the line for Eq. (12b) equals the angle of internal friction, but the slope of the line for Eq. (12a) does not equal the angle of internal friction. This is because the slope is dependent both on the angle of internal friction and on the gradual increase of cohesion with increasing normal stress.

The shear tests have profound implications for strength profiles of lithospheric models, where dry granular material has been used to simulate brittle behaviour of rocks in the lithosphere. In Fig. 7, brittle failure curves (for shortening) have been plotted.

First of all, three curves have been plotted for sand (Ia, b and III), which are the same curves as

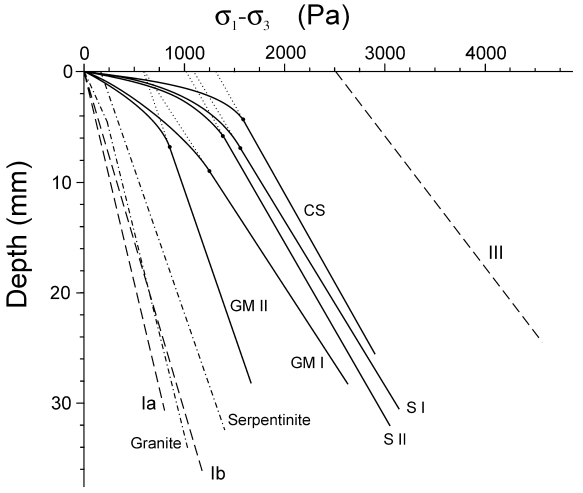

Fig. 7. Brittle failure curves for shortening. The curves numbered Ia,b and III are the same curves as plotted in Fig. 1, except that their densities have been changed. For curve Ia $\rho = 1325$ kg/m^3, for curve Ib $r = 1650$ kg/m^3 and for curve III $\rho = 1780$ kg/m^3. Further, the curves for the investigated materials, S I, S II, GM I, GM II and CS, can be seen. Finally, two curves have been plotted (granite and serpentinite), which are downscaled analogue curves for a granitic crust for a continental lithosphere and a serpentinized olivine upper lithosphere for an oceanic lithosphere. All the curves have been plotted using Eq. (3a), except for granite, which has been plotted using Eqs. (2d) and (2e). For all the curves, the pore fluid factor is 0. From these curves, it can be seen that the strength profiles for the investigated materials are more complex than previously suggested and that their integrated strengths take a position between the two extremes of curves Ia,b and III.

those plotted in Fig. 1, except for their densities. These curves have been plotted using Eq. (3a). For curve Ia, $\rho = 1325$ kg/m^3, for curve Ib, $\rho = 1650$ kg/m^3, and for curve III, $\rho = 1780$ kg/m^3. For curve Ia,b, the densities have been chosen according to the scaling theory (with a density ratio of 1/2 for the analogue model/natural prototype), where curve Ia is the analogue for the continental (granitic) crust, and Ib is the analogue for the upper oceanic (serpentinized olivine) lithosphere. The densities for granite and serpentinized olivine have been taken to be 2650 and 3300 kg/m^3, respectively. The density for curve III is for sprinkled sand from Krantz (1991).

Further, curves have been plotted for the investigated materials S I, S II, GM I, GM II and CS, again by using Eq. (3a).

Finally, two curves have been plotted (granite and serpentinite), which are downscaled analogue curves for a granitic crust for a continental lithosphere and a serpentinized olivine upper lithosphere for an oceanic lithosphere. The curves have been scaled down with a length factor of 10^{-6} (which is often used in analogue lithospheric models) and a density factor of 0.5. These curves represent the scaled down curves (for these scaling factors) to which an ideal brittle analogue material should show a perfect match. Curve granite has been calculated using Eqs. (2d) and (2e) and serpentinite has been calculated using Eq. (3a). This choice of equations has been made since a continental crust is crisscrossed by discontinuities of every shape and size (Ranalli and Murphy, 1987), while an oceanic lithosphere is less deformed compared to a continental lithosphere because the formation and vertical growth of oceanic lithosphere is related to thermal cooling, and normally, an oceanic upper lithosphere has undergone less intensive deformation than continental crust, which grows by intrusions, collision, accretion and underplating. Therefore, the strength of upper continental crust is related to shear resistance of rocks on existing fracture planes, while for upper oceanic lithosphere cohesion plays a more significant role in its strength. For serpentinite, the values of μ and C have been obtained from Table 1. The density of granite and serpentinized olivine has been taken to be 2650 and

Table 5
Integrated strengths for the curves plotted in Fig. 7

Material	Integrated strength (N/m)		
	10 mm	20 mm	30 mm
Ia	1.31	5.23	11.77
Ib	1.63	6.51	14.65
III	29.32	67.90	113.23
S I	~12	~33	~61
S II	~11	~31	~57
GM I	~8	~25	~49
GM II	~7	~19	~34
CS	~14	~37	~65
Granite	2.11	7.06	14.60
Serpentinite	3.57	9.29	18.83

3300 kg/m^3, respectively. Pore fluid pressure has been assumed to be zero in both cases.

From the curves of Fig. 7, it is clear that the integrated strengths for the investigated materials take a position between curves Ia,b and III. The integrated strengths for the curves plotted in Fig. 7 have been given in Table 5 for several thicknesses. Here, it can be seen that the integrated strength increases with increasing thickness. Further, it can be observed that the integrated strength of material GM II shows most resemblance to the integrated strength of curve Ia,b and, more importantly, shows most resemblance to the ideal analogue curves. In particular, the serpentinite curve, with a downscaled cohesion of 45 Pa, shows some resemblance to this analogue material, although the integrated strength of GM II is still too high. However, to a first approximation, it could be a good analogue material with which to model the upper oceanic lithosphere. For larger scale factors, other materials (like S I and S II) might also be appropriate to model the brittle behaviour of the upper lithosphere. However, a disadvantage of these larger scale factors is that the analogue models become extremely large.

6. Conclusions

From the shear tests and normal faulting experiments on various dry granular materials presented above, the following conclusions can be drawn:

1. The coefficient of internal friction and cohesion of the investigated materials are mainly dependent on sphericity and rounding of the individual grains and less dependent on grain size.
2. For normal stresses below a critical value (~250–400 Pa), the failure curves are convex-outward. Above the critical value, the failure curves are straight (Coulomb-type behaviour).
3. The convex shapes of the failure envelopes are associated with a gradual increase in cohesion of the material with increasing normal stress and not with a gradual decrease in coefficient of internal friction, since extensional experiments revealed that there is no significant decrease in fault dip with increasing depth (and thus increasing normal stress on the fault plane).
4. The obtained curves resemble those obtained by Byerlee (1978). The different physical mechanisms operating at different normal stresses, resulting in convex-outward shaped curves for low normal stresses and straight lines for higher normal stresses, are probably comparable with the different physical mechanisms resulting in the two [Eqs. (2b) and (2c)] from Byerlee (1978).
5. Values of cohesion for the investigated materials increase from 0 ($\pm$15 Pa) at $\sigma_n=0$ to 137–247 Pa ($\pm$15 Pa) for $\sigma_n=\sigma_n^*$.
6. The material GM II (fine-grained glass microspheres) is probably the best material to model brittle deformation in the lithosphere, since its integrated strength shows most resemblance to downscaled values of integrated strengths of natural prototype lithospheres (for a length factor of 10^{-6} and a density factor of 1/2). Also, the coefficient of internal friction for GM II ($\mu=0.65$) is (almost) the same as that for granite and serpentinized olivine ($\mu=0.64$ and $\mu=0.65$, respectively). Another advantage is that for fine-grained material, the width of the fault zones and their dilatancy are much more reduced when compared with coarse-grained material, and therefore, it is probably better scaled. Since fine-grained material also provides more structural detail than coarse-grained material, it makes it a better analogue by which to model the brittle behaviour of rocks.

Acknowledgements

I would like to thank Gordon Lister for useful discussions and suggestions to improve the manuscript. Further, the comments of Greg Houseman and Terence Barr were very helpful in improving the manuscript. Also, I would like to thank R.W. Krantz and P.R. Cobbold for reviewing the paper. Finally, thanks go out to Andrew Kos, who helped with recording of some of the experiments. This research was conducted as part of a Ph.D. research at Monash University and was funded by the Smurf 1 grant.

References

Basile, C., Brun, J.P., 1998. Transtensional faulting patterns ranging from pull-apart basins to transform continental margins, an experimental investigation. Journal of Structural Geology 21, 23–37.

Bonini, M., Souriot, T., Boccaletti, M., Brun, J.P., 1997. Successive orthogonal and oblique extension episodes in a rift zone, laboratory experiments with application to the Ethiopian Rift. Tectonics 16, 347–362.

Brun, J.P., Sokoutis, D., van den Driessche, J., 1994. Analogue modeling of detachment fault systems and core complexes. Geology (Boulder) 22, 319–322.

Byerlee, J.D., 1978. Friction of rocks. Pure Applied Geophysics 116, 615–626.

Cobbold, P.R., Jackson, M.P.A., 1992. Gum rosin (colophony): a suitable material for mechanical modelling of the lithosphere. Tectonophysics 210, 255–271.

Cobbold, P.R., Castro, L., 1999. Fluid pressure and effective stress in sandbox models. Tectonophysics 301, 1–19.

Coulomb, C.A., 1773. Sur l'application des régles de maximis et minimis à quelques problèmes de statique, relatifs à l'architecture. Acad. R. Sci. Paris Mem. Math. Phys. 7, 343–382.

Davy, P., Cobbold, P.R., 1988. Indentation tectonics in nature and experiment. 1. Experiments scaled for gravity. Bull. Geol. Inst. Univ. Uppsala, N.S. 14, 129–141.

Davy, Ph., Cobbold, P.R., 1991. Experiments on shortening of a 4-layer model of the continental lithosphere. Tectonophysics 188, 1–25.

Faccenna, C., Davy, P., Brun, J.P., Funiciello, R., Giardini, D., Mattei, M., Nalpas, T., 1996. The Dynamics of back-arc extension: an experimental approach to the opening of the Tyrrhenian Sea. Geophysical Journal International 126, 781–795.

Faccenna, C., Giardini, D., Davy, P., Argentieri, A., 1999. Initiation of subduction at Atlantic-type margins, insights from laboratory experiments. Journal of Geophysical Research 104, 2749–2766.

Handin, J., 1969. On the Coulomb–Mohr failure criterion. Journal of Geophysical Research 74, 5343–5348.

Hatzfeld, D., Martinod, J., Bastet, G., Gautier, P., 1997. An analog experiment for the Aegean to describe the contribution of gravitational potential energy. Journal of Geophysical Research 102, 649–659.

Horsfield, W.T., 1977. An experimental approach to basement-controlled faulting. Geologie en Mijnbouw 56, 363–370.

Hubbert, M.K., 1937. Theory of scale models as applied to the study of geological structures. Bulletin of the Geological Society of America 48, 1459–1520.

Hubbert, M.K., 1951. Mechanical basis for certain geological structures. Bulletin of the Geological Society of America 62, 355–372.

Jaeger, J.C., Cook, N.G.W., 1976. Fundamentals of Rock Mechanics. Chapman & Hall, Wiley, New York, 585 pp.

Keep, M., McClay, K.R., 1997. Analogue modelling of multiphase rift systems. Tectonophysics 273, 239–270.

Kirby, S.H., 1983. Rheology of the lithosphere. Reviews of Geophysics and Space Physics 21, 1458–1487.

Krantz, R.W., 1991. Measurements of friction coefficients and cohesion for faulting and fault reactivation in laboratory models using sand and sand mixtures. Tectonophysics 188, 203–207.

Lallemand, S.E., Malavieille, J., Calassou, S., 1992. Effects of oceanic ridge subduction on accretionary wedges: experimental modeling and marine observations. Tectonics 11, 1301–1313.

Mandl, G., de Jong, L.N.J., Maltha, A., 1977. Shear zones in granular materials. Rock Mechanics 9, 95–144.

Mandl, G., 1988. Mechanics of Tectonic Faulting. Models and Basic Concepts. Elsevier, Amsterdam, 407 pp.

McClay, K.R., 1990. Deformation mechanics in analogue models of extensional fault systems. Geological Society of London Special Publications 54, 445–453.

Naylor, M.A., Mandl, G., Sijpesteijn, C.H.K., 1986. Fault geometries in basement induced wrench faulting under different initial stress states. Journal of Structural Geology 8, 737–752.

Nieuwland, D.A., Walters, J.V., 1993. Geomechanics of the South Furious Field, an integrated approach towards solving complex structural geological problems, including analogue and finite-element modelling. Tectonophysics 226, 143–166.

Powers, M.C., 1953. A new roundness scale for sedimentary particles. Journal of Sedimentary Petrology 23, 117–119.

Raleigh, C.B., Paterson, M.S., 1965. Experimental deformation of serpentinite and its tectonic implications. Journal of Geophysical Research 70, 3965–3985.

Ranalli, G., Murphy, D., 1987. Rheological stratification of the lithosphere. Tectonophysics 132, 281–295.

Ratschbacher, L., Merle, O., Davy, P., Cobbold, P., 1991. Lateral extrusion in the Eastern Alps, part 1: boundary conditions and experiments scaled for gravity. Tectonics 10, 245–256.

Richard, P., 1991. Experiments on faulting in a two-layered cover sequence overlying a reactivated basement fault with oblique-slip. Journal of Structural Geology 13, 459–469.

Richard, P., Krantz, R.W., 1991. Experiments on fault reactivation in strike-slip mode. Tectonophysics 188, 117–131.

Richard, P.D., Moquet, B., Cobbold, P.R., 1991. Experiments on simultaneous faulting and folding above a basement wrench fault. Tectonophysics 188, 133–141.

Richard, P.D., Naylor, M.A., Koopman, A., 1995. Experimental models of strike-slip tectonics. Petroleum Geoscience 1, 71–80.

Sibson, R.H., 1974. Frictional constraints on thrust, wrench and normal faults. Nature 249, 542–544.

Twiss, R.J., Moores, E.M., 1992. Structural Geology. W.H. Freeman and Company, New York, 532 pp.

Vendeville, B., Cobbold, P.R., Davy, P., Choukroune, P., Brun, J.P., 1987. Physical models of extensional tectonics at various scales. Geological Society of London Special Publications 28, 95–107.